

# Demonstration of $\text{In}_{0.9}\text{Ga}_{0.1}\text{As}/\text{GaAs}_{0.18}\text{Sb}_{0.82}$ Near Broken-gap Tunnel FET with $I_{\text{ON}}=740\mu\text{A}/\mu\text{m}$ , $G_{\text{M}}=700\mu\text{S}/\mu\text{m}$ and Gigahertz Switching Performance at $V_{\text{DS}}=0.5\text{V}$

R. Bijesh,\* H. Liu, H. Madan, D. Mohata, W. Li<sup>1</sup>, N. V. Nguyen<sup>1</sup>, D. Gundlach<sup>1</sup>, C.A. Richter<sup>1</sup>, J. Maier, K. Wang, T. Clarke, J. M. Fastenau<sup>2</sup>, D. Loubychev<sup>2</sup>, W. K. Liu<sup>2</sup>, V. Narayanan and S. Datta

The Pennsylvania State University, University Park, PA 16802;

<sup>1</sup>National Institute of Standards and Technology, MD; <sup>2</sup>IQE Inc., Bethlehem, PA;

\*Tel:(814) 954-2391, Email: [bijesh@psu.edu](mailto:bijesh@psu.edu)

**Abstract:** We demonstrate high frequency switching characteristics of TFETs based on the  $\text{In}_{0.9}\text{Ga}_{0.1}\text{As}/\text{GaAs}_{0.18}\text{Sb}_{0.82}$  material system. These near broken-gap TFETs (NBTFETs) with 200nm channel length exhibit record drive current ( $I_{\text{ON}}$ ) of  $740\mu\text{A}/\mu\text{m}$ , intrinsic RF transconductance ( $G_{\text{M}}$ ) of  $700\mu\text{S}/\mu\text{m}$ , and a cut-off frequency ( $F_{\text{T}}$ ) of 19GHz at  $V_{\text{DS}}=0.5\text{V}$ . Numerical simulations calibrated to the experimental data are used to provide insight into the impact of vertical architecture on switching performance of TFETs at scaled technology nodes.

**Introduction:** TFETs can achieve sub-60mV/decade switching slope (SS) at room temperature thereby enabling supply voltage scaling without penalty on the off state leakage. High band to band tunneling (BTBT) current density can be achieved by band-gap engineering [1-2] and implementing near broken gap tunnel barrier in  $\text{In}_{0.9}\text{Ga}_{0.1}\text{As}/\text{GaAs}_{0.18}\text{Sb}_{0.82}$  material system (Fig. 1(a)). Implementing NBTFETs in a vertical architecture provides added advantage in terms of increased device density [3]. In this work, we demonstrate high frequency switching characteristics of NBTFET, for the first time. Through detailed RF characterization coupled with numerical simulations, an optimal vertical NBTFET structure is designed for DC and RF performance with low DC power consumption.

**Materials Characterization:** Fig. 1(b) shows the schematic of the NBTFET layer structure grown by molecular beam epitaxy (MBE). Effective tunnel barrier height ( $E_{\text{b,eff}}$ ) of 0.04eV is expected in NBTFET (Fig. 1(c)). Internal photoemission (IPE) spectroscopy is performed to measure the band-alignment of NBTFETs by using graphene as a transparent electrode (Figs. 2(a)-(d)). The barrier height for holes ( $\Phi_{\text{h}}$ ) from the  $\text{In}_{0.9}\text{Ga}_{0.1}\text{As}$  conduction band (CB) to the  $\text{Al}_2\text{O}_3$  valence band (VB) is found to be 3.05eV from the field independent yield plot (Fig. 2(b)).  $\Phi_{\text{h}}$  for the  $\text{GaAs}_{0.18}\text{Sb}_{0.82}$  CB to the  $\text{Al}_2\text{O}_3$  VB is measured to be 3.72eV (Fig. 2(c)). Within the limits of measurement accuracy, the effective tunneling barrier ( $E_{\text{b,eff}}$ ) of the NBTFET is determined to be 0.02eV with the band-gap of  $\text{GaAs}_{0.18}\text{Sb}_{0.82}$  of assumed to be 0.69eV [4].

**Device Fabrication:** Fig. 3(a) shows the schematic of the vertical NBTFET fabricated by using the process flow described in Fig. 3(b). Implementation of inter-layer dielectric (ILD) and via process technology to contact the sidewall gate and bottom source electrodes reduces the parasitic capacitances, enabling evaluation of the switching characteristics of the vertical NBTFET. The high resolution TEM cross-section image of the fabricated NBTFET shows a sidewall tapering angle of  $53^\circ$ , gate-drain overlap of 120nm and gate-source overlap of 40 nm (Fig. 3(c)).

**DC Characterization:** Fig. 4(a) shows the temperature dependent transfer ( $I_{\text{DS}}-V_{\text{GS}}$ ) characteristics of the NBTFET. The weak observed dependence of  $I_{\text{ON}}$  on temperature is consistent with the band to band tunneling dominated conduction mechanism (Figs. 4(a)-(b)). The NBTFET exhibits  $I_{\text{ON}}=740\mu\text{A}/\mu\text{m}$  at  $V_{\text{GS}}=2.5\text{V}$ ,  $V_{\text{DS}}=0.5\text{V}$ . Saturation is observed in the output characteristics at lower  $V_{\text{GS}}$  range; however, for higher  $V_{\text{GS}}$ , series resistance affects the saturation characteristics. At  $T=300\text{K}$ ,  $V_{\text{DS}}=0.5\text{V}$  the NBTFET exhibits peak extrinsic DC  $G_{\text{M}}$  of  $680\mu\text{S}/\mu\text{m}$  (Fig. 4(c)). Activation energy of 0.21eV is obtained from the Arrhenius plot in Fig. 4(d), which is close to half of the band-gap ( $E_{\text{g}}$ ) of  $\text{In}_{0.9}\text{Ga}_{0.1}\text{As}$  indicating a SRH dominated leakage floor ( $I_{\text{OFF}}$ ). InAs homo-junction p-i-n diodes fabricated for comparison showed significantly lower  $I_{\text{OFF}}$  (Fig. 4(d)). Hence, the  $I_{\text{OFF}}$  in NBTFET at  $T=300\text{K}$  is attributed to SRH generation-recombination current arising from a high density of defect states.

**Pulsed-IV Characterization:** Numerical simulation is calibrated with the measured  $I_{\text{DS}}-V_{\text{GS}}$  characteristics at  $T=300\text{K}$ ,  $V_{\text{DS}}=0.5\text{V}$  by introducing interface states density ( $D_{\text{it}}$ ) of  $5 \times 10^{12} \text{cm}^{-2}\text{eV}^{-1}$ . The electron quasi Fermi level in the channel is obtained from numerical simulation and is found to move from deep inside the CB in the on-state to near mid-gap (MG) as  $V_{\text{GS}}$  is reduced until bulk leakage currents dominate the electrical characteristics (Fig. 5(a)). 100ns gate pulsing suppresses  $D_{\text{it}}$  response in the energy range from MG to 0.1eV farther from MG, whereas  $1\mu\text{s}$  gate pulsing suppresses  $D_{\text{it}}$  response in the energy range only 0.035 eV farther from MG (Fig. 5(b)). Fig. 5(c) shows the  $I_{\text{DS}}-V_{\text{GS}}$  characteristics at  $V_{\text{DS}}=0.5\text{V}$  for varying gate voltage pulse widths. Fig. 5(d) shows the corresponding SS as a function of drain current. SS is found to improve with faster gate voltage pulsing and further improves with reduction in  $I_{\text{OFF}}$  ( $T=77\text{K}$ ) and EOT scaling.

**RF Characterization:** A coplanar ground-signal-ground (GSG) waveguide structure is used to inject RF signal into the NBTFET (Fig. 6(a)). Fig. 6(b) shows the measured and modeled scattering parameters of NBTFET from 40MHz to 20GHz which are in excellent agreement with each other. Fig. 6(c) shows the measured and modeled small signal current gain,  $h_{21}$  as a function of frequency. The 200nm  $L_{\text{ch}}$  NBTFET exhibits  $F_{\text{T}}$  of 10GHz and 19GHz at  $V_{\text{DS}}=0.3\text{V}$  and  $0.5\text{V}$  (RF  $G_{\text{M}}=700\mu\text{S}/\mu\text{m}$ ) respectively. Numerical simulation of the NBTFET structure matched to the HRTEM image is carried out taking into account the various parasitic capacitances and resistances (Figs. 7(a-b)) [3]. Simulated  $C_{\text{gs,extrinsic}}$  and  $C_{\text{gd,extrinsic}}$  values are in agreement with the measured values from the RF measurements (Figs. 8(a-d)).  $C_{\text{gs,ov}}$  and  $C_{\text{gd,ov}}$  are the dominant parasitic capacitances which when de-embedded result in  $F_{\text{T}}$  of 22GHz and 39GHz

at 0.3V and 0.5V  $V_{DS}$  respectively (Figs. 9(a)-(b)). Further, gate-drain overlap results in increased gate capacitance ( $C_{gg,extrinsic}$ ) as well as reduced series resistance corresponding to improved  $G_M$ . NBTFTs with a gate-drain underlap of 40 nm deliver maximum  $F_T$  (Figs. 10(a-b)). Figs. 10(c-e) show the impact of the sidewall tapering angle on the switching performance of TFTs. Increased gate capacitance due to tapering is countered by improved  $G_M$  arising from the longer spread of BTBT generated carriers. An optimum tapering angle of  $80^\circ$  maximizes  $F_T$ . Vertical NBTFT with scaled dimensions (Table I) are found to outperform both the DC and RF performance of 32nm CMOS (Figs. 11 (a-c)).

**Conclusion:** 200 nm  $L_{ch}$  NBTFTs have been demonstrated with record high  $I_{ON}=740\mu A/\mu m$ , RF  $G_M=700\mu S/\mu m$  and  $F_T=19$  GHz. Vertical NBTFTs with scaled device dimensions, optimized gate-source overlap, gate-drain underlap, and sidewall tapering angle outperform CMOS in terms of both DC and RF characteristics with lower DC biasing power.

**Acknowledgments:** This work was supported in part by the NRI/SRC sponsored MIND center and by the National Science Foundation ASSIST Nanosystems ERC under Award Number EEC- 1160483.

**References:** [1] D. Mohata, R. Bijesh, S. Mujumdar, C. Eaton, R. Engel-Herbert, T. Mayer, V. Narayanan, J. M. Fastenau, D. Loubichev, A. K. Liu and S. Datta, *IEDM Tech. Digest*, pp. 33.5.1-33.5.4 (2011). [2] D. Pawlik, B. Romanczyk, P. Thomas, S. Rommel, M. Edirisooriya, R. Contreras-Guerrero, R. Droopad, W-Y Loh, M. H. Wong, K. Majumdar, W.-E Wang, P. D. Kirsch, and R. Jammy, *IEDM Tech. Digest*, pp. 812-814, (2012) [3] H. Liu, D. K. Mohata, A. Nidhi, V. Saripalli, V. Narayanan and S. Datta, *DRC Tech. Digest*, pp. 233-234, (2012). [4] I. Vurgaftman, J. R. Mayer and R. Ram-Mohan, *J. Appl. Phys.* 89, 5815 (2001). [5] P. VanDerVoorn, M. Agostinelli, S.-J. Choi, G. Curello, H. Deshpande, M. A. El-Tanani, W. Hafez, U. Jalan, L. Janbay, M. Kang, K.-J. Koh, K. Komeyli, H. Lakdawala, J. Lin, N. Lindert, S. Mudanai, J. Park, K. Phoa, A. Rahman, J. Rizk, L. Rockford, G. Sacks, K. Soumyanath, H. Tashiro, S. Taylor, C. Tsai, H. Xu, J. Xu, L. Yang, I. Young, J.-Y. Yeh, J. Yip, P. Bai, and C.-H. Jan, *VLSI Tech. Digest*, pp. 137-138 (2010).

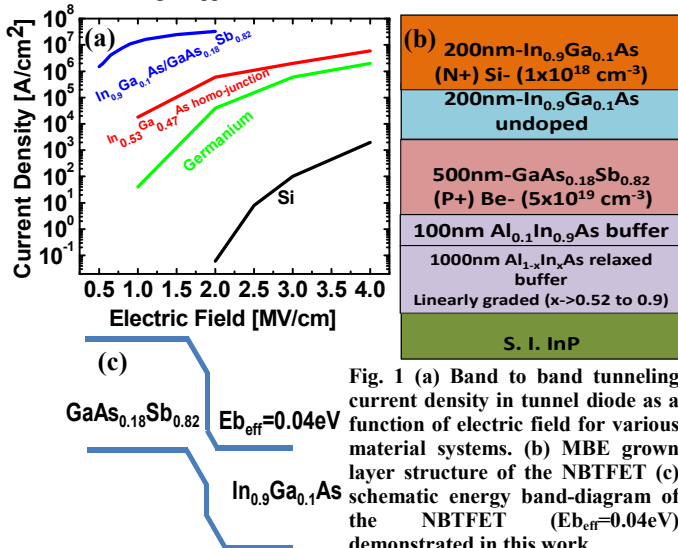


Fig. 1 (a) Band to band tunneling current density in tunnel diode as a function of electric field for various material systems. (b) MBE grown layer structure of the NBTFT (c) schematic energy band-diagram of the NBTFT ( $E_{b,eff}=0.04eV$ ) demonstrated in this work.

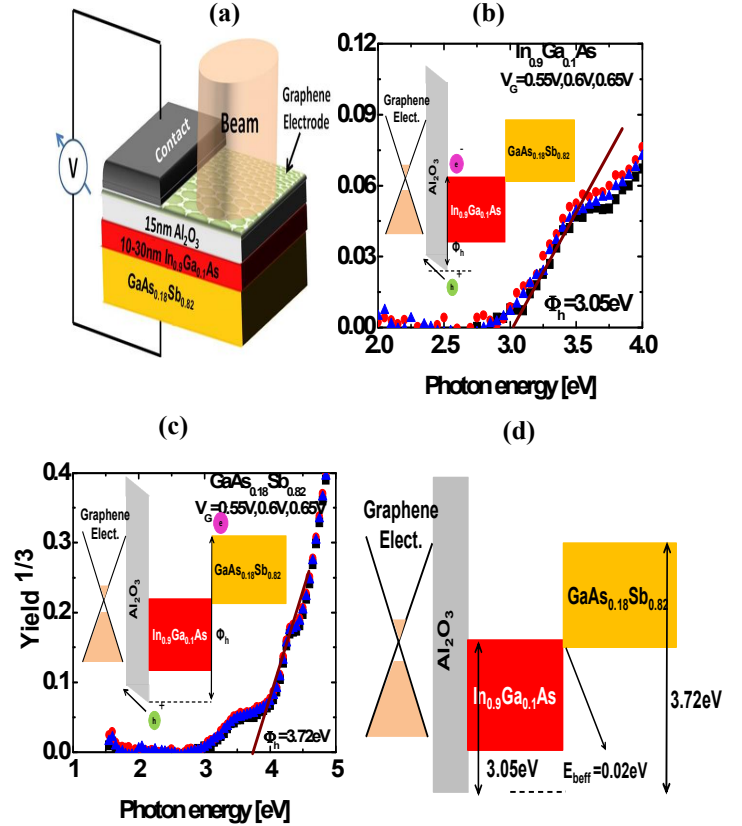


Fig. 2 (a) Internal photo emission spectroscopy experiment setup using graphene as a transparent electrode. (b) Barrier height for hole emission from  $In_{0.9}Ga_{0.1}As$  is measured to be 3.05eV. (c) Barrier height for hole emission from  $GaAs_{0.18}Sb_{0.82}$  is measured to be 3.72eV. (d) The as-grown NBTFT has an effective barrier height of 0.02eV.

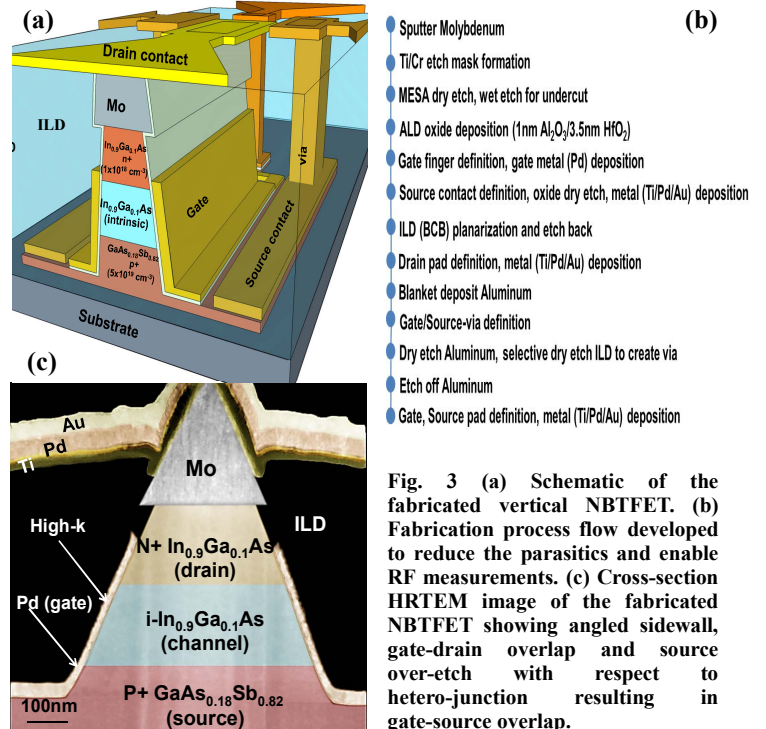


Fig. 3 (a) Schematic of the fabricated vertical NBTFT. (b) Fabrication process flow developed to reduce the parasitics and enable RF measurements. (c) Cross-section HRTEM image of the fabricated NBTFT showing angled sidewall, gate-drain overlap and source over-etch with respect to hetero-junction resulting in gate-source overlap.

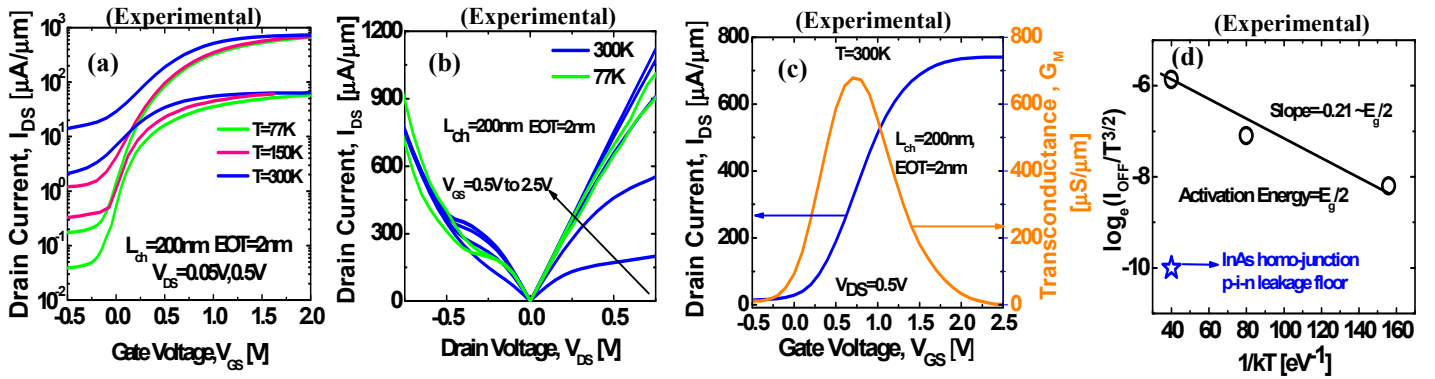


Fig. 4 (a) Temperature dependent transfer characteristics of NBTFT showing improved  $I_{ON}/I_{OFF}$  at low temperature. (b) Output characteristics of NBTFT at  $T=300K$  and  $T=77K$ . (c) NBTFT exhibits peak extrinsic  $G_m$  of  $680\mu S/\mu m$  at  $T=300 K$ ,  $V_{DS}=0.5V$ . (d) Activation energy of  $E_g/2$  confirms SRH generation-recombination in  $In_{0.9}Ga_{0.1}As$  as the mechanism setting  $I_{OFF}$ . InAs homojunction p-i-n leakage floor at  $T=300K$  is much lower in comparison.

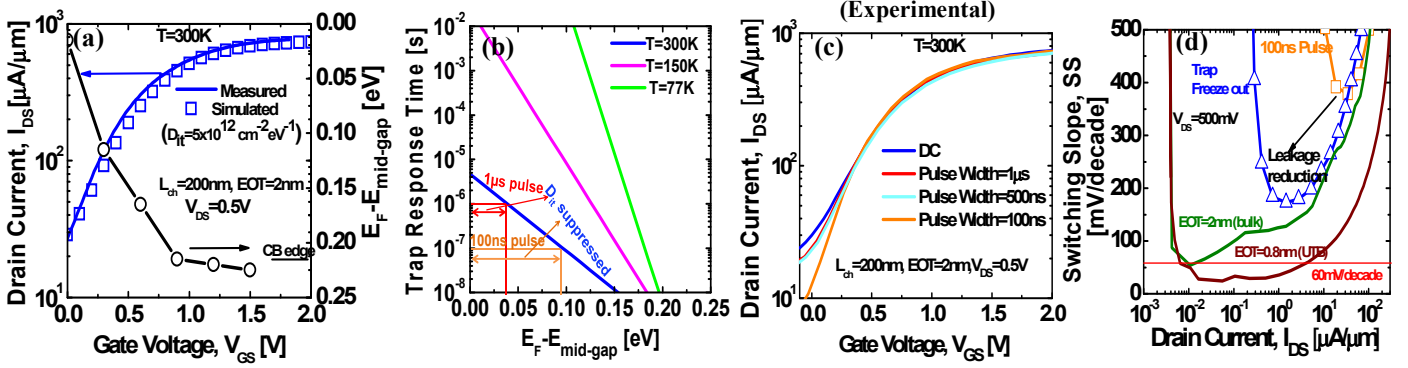


Fig. 5 (a) Numerical simulation calibrated to measured  $I_{DS}$ - $V_{GS}$  characteristics at  $T=300K$  is used to map the electron quasi-Fermi level movement in the channel (b) Simulated electron trap response time in  $In_{0.9}Ga_{0.1}As$  is used to estimate the gate voltage pulse width required to suppress  $D_{it}$  response. (c) Transfer characteristics at  $T=300K$ ,  $V_{DS}=0.5V$  for varying gate pulse widths. (d) SS as a function of drain current at  $V_{DS}=0.5V$  showing improvement with pulsing, reduction in leakage floor and EOT scaling.

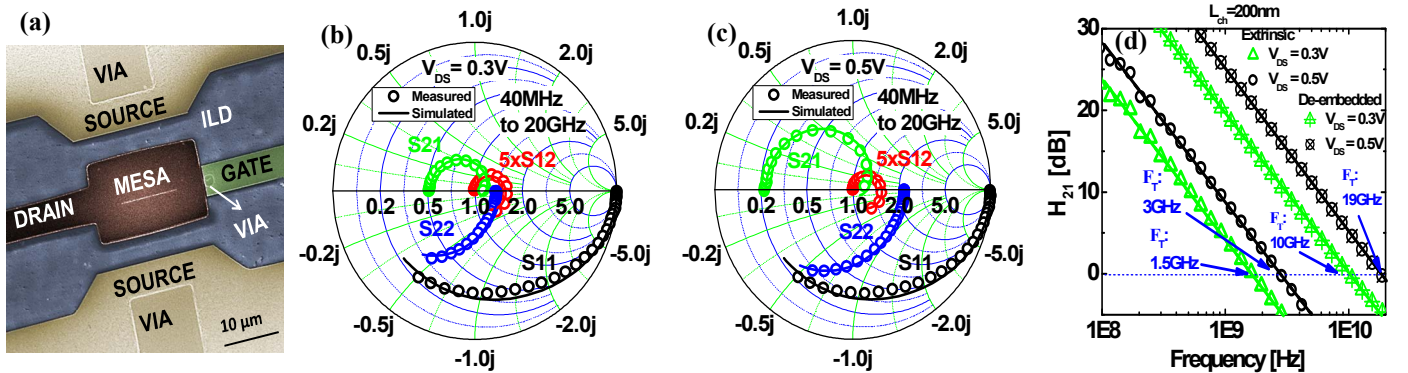


Fig. 6 (a) SEM image of the fabricated NBTFT under GSG configuration. (b-c) Modeled and measured s-parameters at  $V_{DS}=0.3V$  and  $0.5V$  respectively. (d) Measured and modeled  $H_{21}$  parameter at  $V_{DS}=0.5V$  and  $0.3V$ . After de-embedding,  $F_T$  of  $10GHz$  and  $19GHz$  are measured at  $V_{DS}=0.3V$  and  $0.5V$  respectively. RF  $G_m=700\mu S/\mu m$  is measured at  $V_{DS}=0.5V$ .

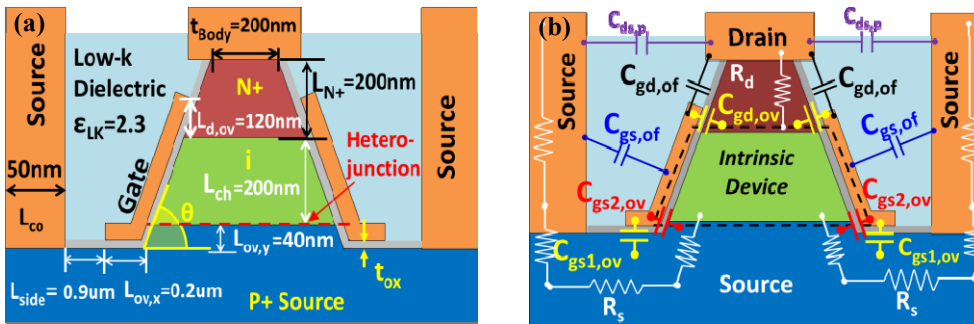


Fig. 7 (a) 2D schematic of the NBTFT used to perform numerical simulation. The geometric parameters were obtained from the HRTEM image of the NBTFT shown in fig. 3(c). (b) Illustration of the parasitic resistances and capacitances taken into consideration for numerical simulation of the NBTFT to evaluate the RF performance.



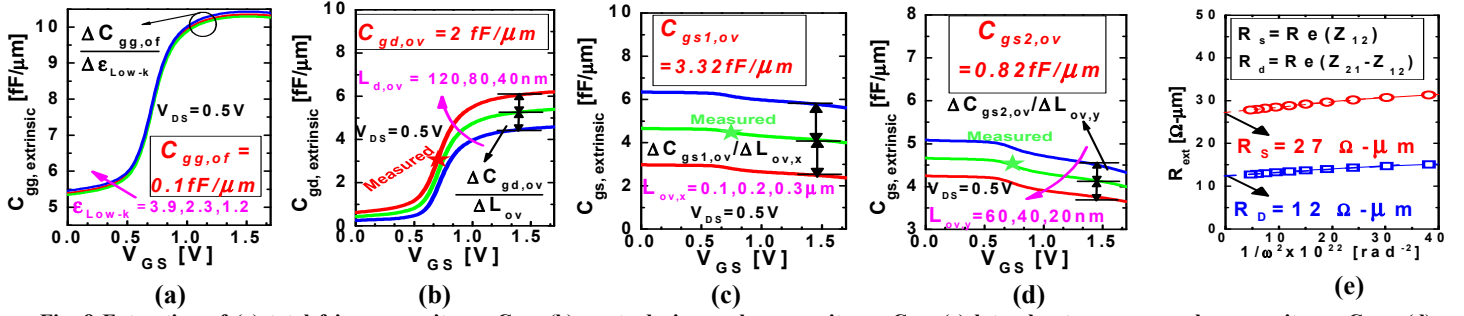


Fig. 8 Extraction of (a) total fringe capacitance  $C_{gg,of}$  (b) gate-drain overlap capacitance  $C_{gd,ov}$  (c) lateral gate-source overlap capacitance  $C_{gs1,ov}$  (d) gate-source overlap capacitance along the sidewall  $C_{gs2,ov}$  (e) series resistances  $R_s$  and  $R_d$ .

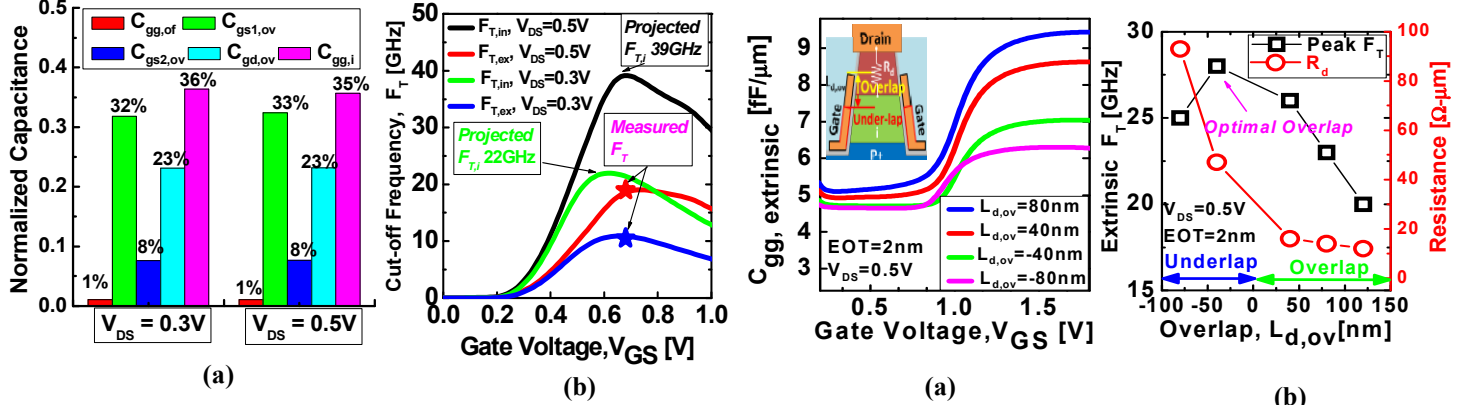


Fig. 9 (a) Percentage contribution of various capacitance components at  $V_{DS}=0.3V$  and  $0.5V$  showing the dominance of gate-source and gate-drain overlap capacitances. (b) Measured  $F_T$  is in agreement with the simulations. After de-embedding the overlap capacitances, NBTFT with  $L_{ch}=200nm$  is expected to achieve  $F_T$  of 22GHz and 39GHz at  $V_{DS}=0.3V$  and  $0.5V$  respectively.

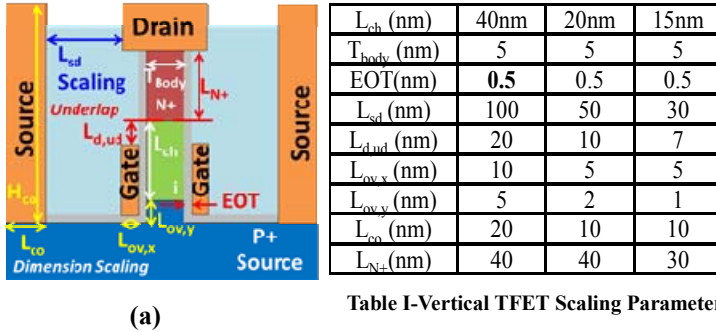


Table I-Vertical TFET Scaling Parameters

	40nm	20nm	15nm
$L_{ch}$ (nm)	40nm	20nm	15nm
$T_{body}$ (nm)	5	5	5
EOT(nm)	0.5	0.5	0.5
$L_{sd}$ (nm)	100	50	30
$L_{d,ud}$ (nm)	20	10	7
$L_{ov,x}$ (nm)	10	5	5
$L_{ov,y}$ (nm)	5	2	1
$L_{on}$ (nm)	20	10	10
$L_{N+}$ (nm)	40	40	30

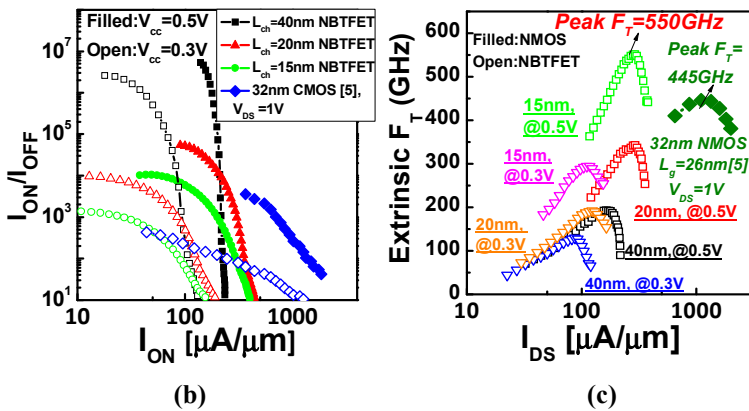


Fig. 11 (a) Schematic of the scaled NBTFT, the device parameters are shown in table I. (b)  $I_{ON}$  vs  $I_{ON}/I_{OFF}$  plot of the NBTFT for different  $L_{ch}$  compared to 32nm CMOS. (c) Comparison of the projected extrinsic  $F_T$  of NBTFT compared to 32nm CMOS.

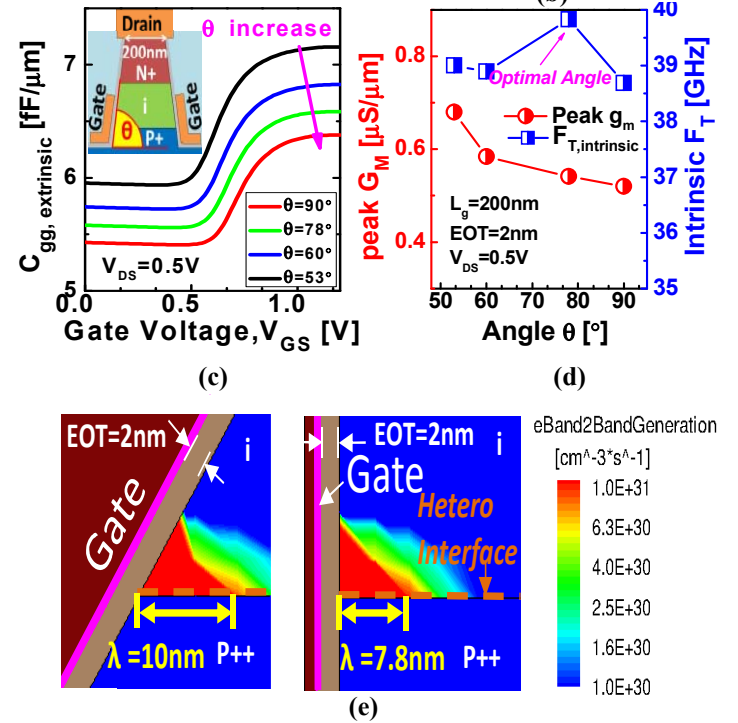


Fig. 10 (a) Extrinsic gate capacitance,  $C_{gg}$  as a function of the gate bias showing increase with increasing gate-drain overlap. Inset shows the schematic of the structure simulated (b) The drain side series resistance  $R_d$  reduces with increased gate-drain overlap, however due to increase in  $C_{gg}$  with gate-drain overlap, overall extrinsic  $F_T$  is found to be optimum at underlap of 40nm. (c)  $C_{gg}$  as a function of gate bias showing increase in magnitude as the sidewall becomes more tapered. Inset shows the schematic of the structure simulated (d) Peak  $G_m$  reduces as the etched sidewall becomes less tapered, with intrinsic  $F_T$  optimum corresponding to  $\theta=80^\circ$  (e) The spread in the electron band to band generation rate is higher with a tapered sidewall giving rise to increased peak  $G_m$ .